Deformable B-Solids: Application for Localization and Tracking of MRI-SPAMM Data

Petia Radeva, Amir Amini*†, Jiantao Huang† and Enric Martí

UPIIA, Departament d'Informatica,
Universitat Autonoma de Barcelona, Bellaterra (Barcelona), SPAIN

Departments of *Diagnostic Radiology and †Electrical Engineering,
Yale University, New Haven, CT 06520, US
e-mail: petia,enric@upisun1.uab.es, amini,wangjz@minerva.cis.yale.edu

Abstract

The development of MR tagging techniques has allowed for estimation of local 3D motion of the heart's endocardial and epicardial boundaries as well as transmural cardiac deformations. For analysis of tag data, to date, data from different image slices have been considered independently. In this paper, we propose an approach for 3D tag localization and tracking of MRI-SPAMM data by a novel deformable B-solid. The solid is defined in terms of a 3D tensor product B-spline which we require to be aligned with tag lines from different image slices. The localization and tracking of tag lines is performed under constraints of continuity and smoothness, taking into account that tag lines belong to the same deformable body. Analyzing the deformation of 3D tags unifies the problem of localization, and displacement fitting and interpolation into the same procedure. To track endocardial and epicardial motion, a volumetric heart model is employed which is a pair of coupled endocardial and epicardial B-spline surfaces. In order to recover heart's deformations, an energy-minimization problem is posed where both tag and heart boundary data are used. The framework allows for integration of tag data from Short Axis (SA) and Long Axis (LA) tagged cardiac images.

Keywords: snakes, deformable solids, deformable models, SPAMM-MRI

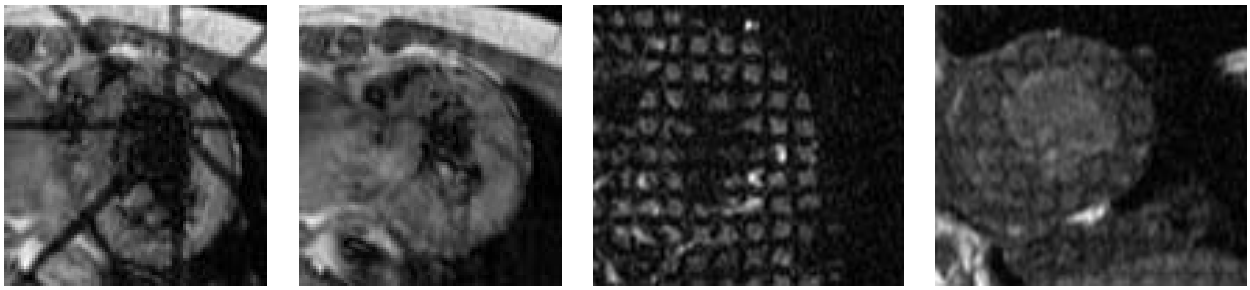

a b c d

Figure 1: Radial (a,b) and SPAMM (c,d) tag images of short axes views taken in diastole (a,c) and systole (b,d) stage of the cardiac cicle

1 Introduction

Non-invasive techniques for assessing the dynamic behavior of the human heart are invaluable in the diagnosis of heart disease, as abnormalities in the myocardial motion sensitively reflect deficits in blood perfusion [9]. MRI is an excellent imaging technique for measuring non-rigid tissue motion, as it is capable of selectively altering material property of the underlying tissue (magnetization in this case), in order to create tagged patterns within a deforming body such as the heart muscle. The resulting pattern defines a time-varying curvilinear coordinate system on the tissue (see Fig. 1).

Several tagged imaging techniques have been proposed in the MR literature. The basic premise in all tagging schemes involves using a set of RF pulses to place tags in thin slices of the myocardium, perpendicular to the imaging plane which can then be tracked over the heart cycle. The method originally proposed by Elias Zerhouni in 1988 [36] (star-burst tagging) produces a number of radial saturation stripes within the image (see Fig. 1(a) and (b)). SPAMM[4] is a technique for producing a grid pattern of signal voids on the tissue – two perpendicular sets of tagging planes, each perpendicular to the imaging plane (see Fig. 1(c) and (d)). We have chosen to concentrate on SPAMM for measurement of deformations because a number of points can be marked in a very short time and tracked, providing the means for obtaining 3D correspondence of material points over time.

Accurate detection of tags is crucial to measurement of deformations and understanding of myocardial function. In [33], tag intersections are located by a semi-automated process. In [2, 3, 13, 16] detection of tag stripes is performed by graph search and tag profile fitting. In order to determine the tag locations, tag profiles are simulated as a function of time using physics of MRI. The profile fitting approach has been improved by utilizing a template matching procedure in [1, 2, 3], or by additional local analysis [21, 13]. In [1, 34, 17], authors have adopted a 2D snake analysis system for different image slices in order to recover within slice tag motion. Their approach aims to minimize an external energy which is the sum of intensities for each slice, together with an internal energy which provides smoothness. As pointed out in [17], detection of tag data with varying contrast needs spatially varying parameters for snakes, making automated localization non-trivial. Other approaches to capture heart motion is based on optical flow analysis of tagged MRI [28, 12]. To provide satisfactory results knowledge is required about different imaging parameters (T_1, proton density,...) in the region of interest. New work on application of optical flow to tagged imagery has resulted in algorithms not requiring tissue specific and imaging parameters [12].

Our goal in this work is to develop a model for detection of local deformations of the

heart based on tag and contour data. We continue the previous approach of detecting locally deforming tag stripes using 2D deformable grids [1, 2, 3, 34] and show how this analysis can be extended to 3D. We employ a planar surface description for the tag planes in the form of deformable iso-parametric surfaces of a B-solid, and provide the necessary smoothness constraints required in robust localization of tag information. Such an extension is justified by the fact that different slices represent parts of the same continuous body. In particular, tag lines appearing in different slices belong to continuous tag planes and thus should satisfy smoothness constraints. Hence, deformation of tag grids from different slices should be jointly considered. As an additional point, inhomogeneities in T_1 of myocardial tissue leads to different tag points being visible up to different times (see Fig. 1). The propagation of information across slices will help with such data analysis issues.

The B-solid is implemented as a 3D tensor product B-spline model. This is a compact model, yet it is flexible enough to follow the movement of the heart with high accuracy. Its compactness is due to the fact that the solid is completely defined by a set of control points much smaller in number than the number of voxels in the volume. In the deformable B-solid, two sets of iso-parametric surfaces are aligned with parallel lines of tag grids from the sequence of short axis images. A set of iso-parametric curves links the tag intersections from the different slices. We refer to the curves which are formed from intersection of iso-parametric surfaces with image slices as implicit snakes.

To date, tag detection and estimation of three-dimensional local deformation have been considered as two separate procedures. Usually, the second step corresponds to constructing a volumetric heart model using information from tags and contours. Such volumetric models are: generalized volumetric finite element elliptical model [27], prolate spheroidal model [35, 24], generalized periodic cylindrical model [24], and hybrid volumetric ventriculoid [25]. All of these are designed to perform a global fit with the heart contours and deform in accordance with the tag data displacements. As a byproduct of representing the tags by implicit snakes, localization and displacement fitting and interpolation of tag information are performed in a single procedure. In attracting these curves to tag data, appropriate external forces are defined, adjusting the B-solid, and hence tracking the local deformation of the tissue. In this paper, we consider only SA image slices, and as such consider external forces from the image planes which alter the position of the implicit snakes within image slices. In contrast to external forces, three dimensional internal forces are applied to the B-solid.

A common feature of most heart motion reconstruction schemes (including volumetric heart model) is that they use sparse information provided only by tag intersections [33, 35, 27] or intersections between tags and myocardial contours to detect the local deformation of the heart tissue. Analysis with such sparse tag data neglect valuable information contained at other locations along tag lines. In relation to volumetric-based models, the B-solid uses all the information contained in tag displacements. It is worthwhile to mention that the B-solid has no parameters to adjust except the parameters of elasticity of the implicit snakes. Moreover, B-spline models are more flexible than the available ones, since local estimation of the tag displacements are not affected by strong constraints imposed by the model.

Improvements are also proposed in this paper, for snake analysis of tag data. In particular, the usual internal forces are modified in a way to preserve characteristics of an ideal B-solid. As a consequence, the shrinking problem of the snakes which is commonly encountered is bypassed. To provide a contrast-independent detector for dark tag bands, we construct directional potential fields for implicit snakes from principal

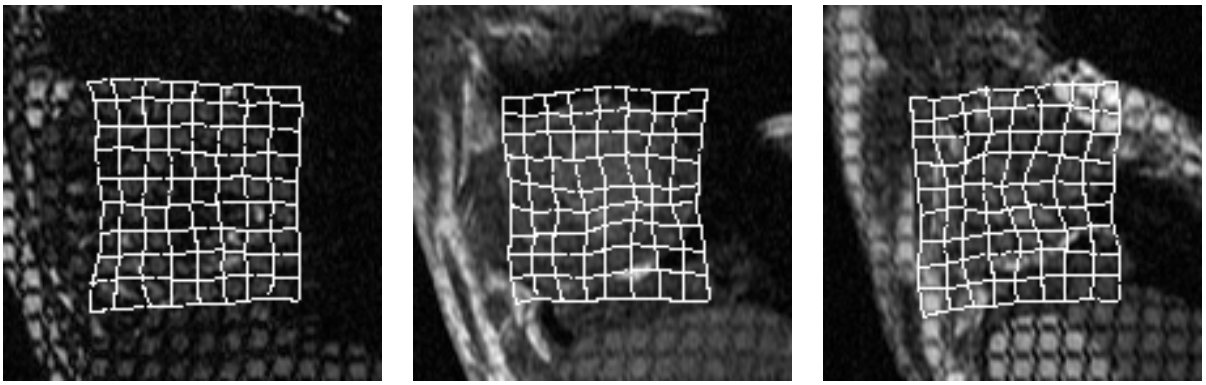

a b c

Figure 2: Localization of tags by B-solid: tag grids detected by implicit snakes of the B-solid

curvature features of tagged images. To achieve high presicion for tag detection, the curvatures of the tagged images are computed by applying Haralick's facet model [14]. The directional sensitivity of the potentials has the advantage that implicit snakes are attracted only by tag lines which have similar orientations.

In addition to the deformable B-solid, we consider a B-spline representation for the heart boundaries, attached to the B-solid. The deformable B-spline heart model possesses local control, allowing the representation to better adjust to the data and interpolate the contours providing an accurate representation for the heart. In contrast, most of the available models [27, 35, 25] are designed to perform a global fit to the heart contours, and hence can at best roughly approximate the contours. Furthermore, global least-square fits are not robust against noise. The reason for our utilizing the heart surfaces is first, to restrict the analysis of deformations to the heart tissue, avoiding the influence of regions around the heart, and second to take into account the information provided by the deforming epicardial and endocardial boundaries of the heart, without an unnecessary effort to provide local correspondence of points. In the process of tracking, we use the fact that the B-solid and heart boundaries correspond to material points of the same tissue, and define a procedure to minimize the energy of the B-solid with external forces from tag and contour data acting on the B-solid.

The rest of the paper is organized as follows: section 2 introduces the deformable B-solid, section 3 discusses energies associated with the deformable B-solid, sections 4 and 5 define the localization by the deformable B-solid and heart model respectively, and section 6 considers the tracking problem for the deformable B-solid. In section 7 an extension of the B-solid approach to SA and LA images analysis is outlined and finally, conclusions are given.

2 Deformable B-Solid

In this section, we discuss implicit snakes and the B-solid. As will be described, implicit snakes track the deformations resulting from the tag data. A heart model will be described which is designed to track the endocardial and epicardial heart boundaries, and is attached to the B-solid. The use of two models is found to be necessary in order to achieve high precision in representing both tag and contour structures.

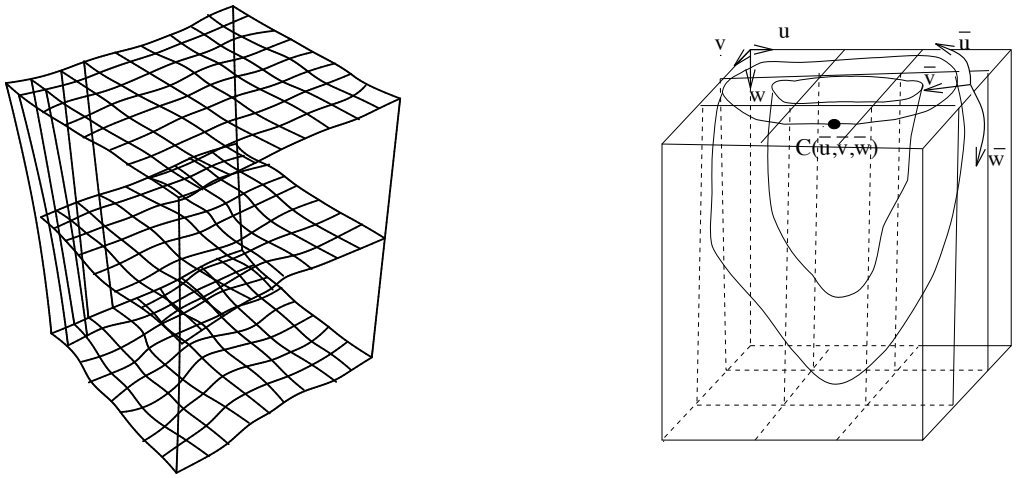

a b

Figure 3: Constructing B-solid from tag lines in imaging planes (a) and coordinate systems of B-solid $(u-v-w)$ and heart model $(\bar{u}-\bar{v}-\bar{w})$ (b) (see text)

2.1 Definition of Deformable B-Solid

We define the B-solid as a 3D tensor product B-spline with the tagging and imaging planes corresponding to the iso-parametric surfaces of the B-spline (see Fig. 2). The B-solid has all the attractive properties of B-spline curves and surfaces: (1) B-splines provide local control of shape, allowing for exactly fitting the deformed tag planes. In addition, individual movement of control points will only affect the solid's shape locally. (2) Cubic B-splines possess second order continuity everywhere. In addition, due to parametric continuity, representing tag lines with B-splines will allow for sub-pixel localization of the tag features. (3) The degree of B-spline blending polynomials is independent of the number of control points, and furthermore the solid is completely specified by few control points.

To describe a solid in 3D, we define the tensor product,

$$Q(u,v,w) = \sum_{i=0}^{I}\sum_{j=0}^{J}\sum_{k=0}^{K} S_{kji}B_i(u)B_j(v)B_k(w),$$

where $B_i(u)$, $B_j(v)$ and $B_k(w)$ are the blending B-spline functions and $S_{kji}, k = 0,...K, j = 0,...J, i = 0,...I$, are the control points of the B-solid. Our implementation assumes non-periodic cubic splines, though our approach is valid for any other spline degrees. Cubic B-splines have an optimal approximation property, namely, that among all interpolants they minimize the norm of the second derivative [23, 10]. As we will consider thin-plate energy of the B-solid in our enery-based formulation, it is reasonable to construct the deformable model with a cubic degree.

In a short axis acquisition, the u and v iso-parametric surfaces are aligned with tag planes, and the $u-v$ iso-parametric curves link the tag intersections from the different slices (see Fig. 2 and Fig. 3 (a)). Thus, the u and v iso-parametric planes deform with the tag planes and w - with the SA imaging plane (or LA tag planes). Without loss of generality, we assume that the tag planes are parallel to the coordinate axes. Assuming

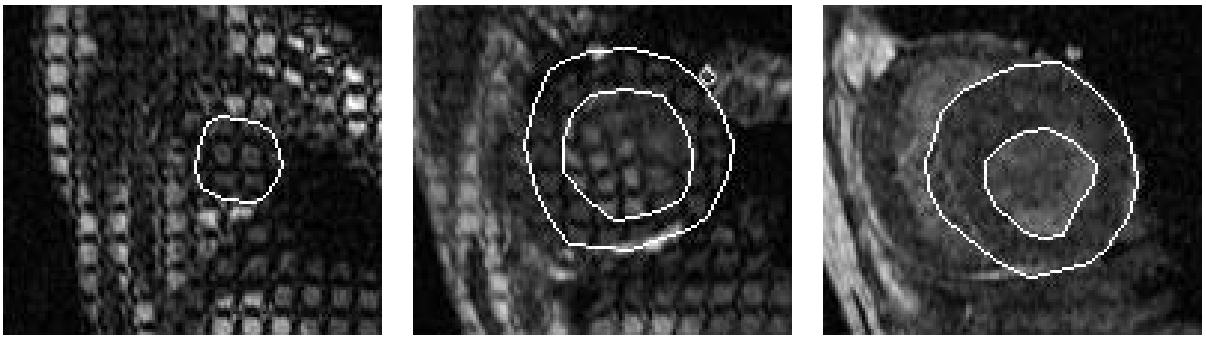

a b c

Figure 4: Heart contours

that at the initial moment the tag planes are flat, it follows that the coordinate axes (x, y, z) are oriented parallel to the $(u - v - w)$ coordinates in the first volumetric image frame.

2.2 Heart Model

Our strategy in analysis of tag data incorporates information about the heart motion from two different sources: tag data as well as heart boundaries. Given the epicardial and endocardial surfaces of the heart, we can represent this information as a pair of coupled boundary surfaces of the endocardium and epicardium using tensor product B-splines:

$$H(x, y, z) = \sum_{o=0}^{O} \sum_{p=0}^{P} \sum_{q=0}^{Q} H_{qpo} B_o(\bar{u}) B_p(\bar{v}) B_q(\bar{w})$$

where H_{qpo} are the control points and $(\bar{u}, \bar{v}, \bar{w})$ are the coordinates of the heart model. The $\bar{u}$ iso-parametric curves coincide with the inner and outer contours from each slice and, due to the closed curves, the corresponding blending functions are periodic. The $\bar{v}$-iso-parametric curves link the epicardial and endocardial contour from each slice, and the $\bar{w}$-iso-parametric curves go through the contours from the different slices (see Fig. 3 (a)). Their corresponding classes of blending functions are non-periodic. Defined in this way, the model has a volumetric cylindrical shape. To consider the complete shape from apex to base, we can place multiple knots at apex, hence creating the oval shape of the LV.

Non-linear blending functions of the parameters $\bar{u}$ and $\bar{w}$ give a realistic shape to the heart. As for the parameter $\bar{v}$, we have used linear spline functions. This is because our heart model is in fact a coupled boundaries model containing information only from the epicardial and endocardial surfaces. In Fig. 5 both surfaces that construct the volumetric heart model derived from heart contours given in Fig. 4 are shown. In Fig. 6 (a) a volumetric heart model located in a B-solid is shown. Note that this model allows to the user to see at different interections (SA and LA) the movement of the heart boundaries and the transmural local deformation (see Fig. 6 (b) and (c)).

2.3 Relation between Tag and Heart Models

In this section we will show how we can express points of the heart model as functions of the parameters of the tag model. This will be a required step in integrating the tags and contours in our framework. Let the point $C(\bar{u}, \bar{v}, \bar{w}) = (x, y, z)$ be a control point

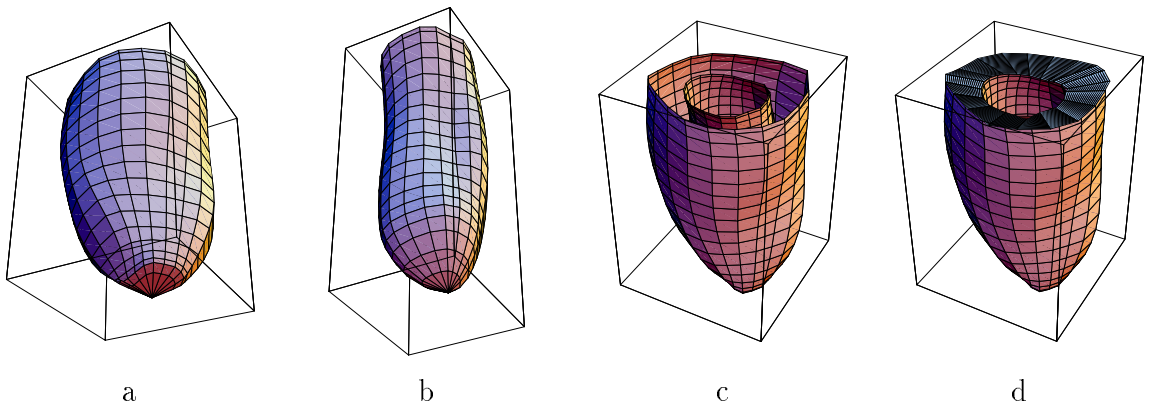

Figure 5: Heart outer (a) and inner (b) boundaries, coupled boundaries (c) and heart volumetric model (d) represented by B-splines

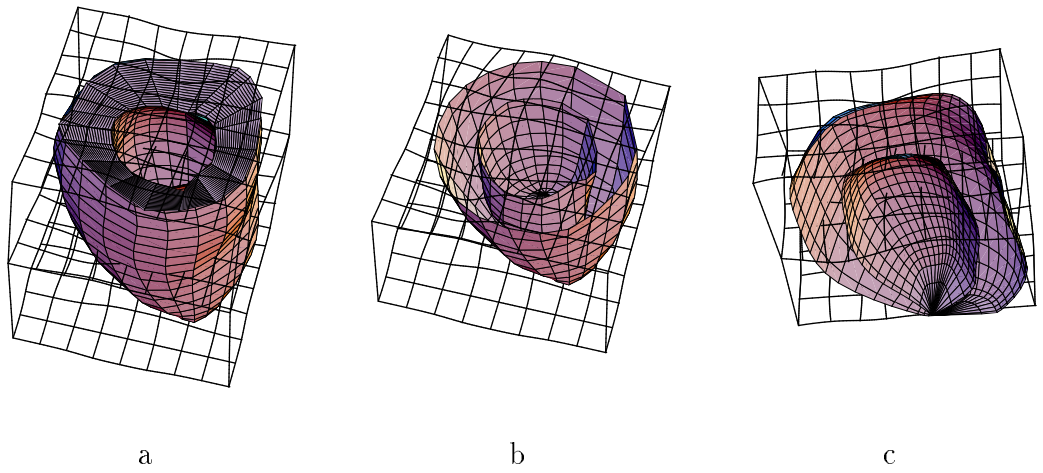

Figure 6: Heart volumetric model located in a B-solid (a), SA (b) and LA (c) intersections of the B-solid

in the heart model (see Fig. 3 (b)). We need to find the parameters $(\tilde{u}, \tilde{v}, \tilde{w})$ from the B-solid so that $C = \sum_{i=0}^{I} \sum_{j=0}^{J} \sum_{k=0}^{K} S_{kji} B_i(\tilde{u}) B_j(\tilde{v}) B_k(\tilde{w})$, where S_{kji} are the control vertices of the tag model. We have a three-dimensional problem with two cubic splines, and hence the relationship between the two sets of coordinates will require solution of an equation of degree 6 resulting in a complex procedure.

As an alternate scheme, we propose a two step procedure for relating the parameters of the heart and tag models. The first step consists of solving the system,

$$C = \sum_{i=0}^{I} \sum_{j=0}^{J} \sum_{k=0}^{K} S_{kji} B_i^1(u) B_j^1(v) B_k^1(w) \tag{1}$$

where B^1 are linear spline blending functions of the parameters of the B-solid and S_{kji} are the control vertices of the B-solid. It is not difficult to see that (1) consists of three tri-linear equations involving each of the parameters (u, v, w), and hence is easy to solve. A solution always exists since point C belongs to an area of the B-solid. The parameter $w = w_0$ is determined directly from the fact that the point C belongs to an imaging (and thus, iso-parametric) plane. The resulting bi-linear system for the parameters (u, v) is [22],

$$(v \quad 1) \begin{pmatrix} -1 & 1 \\ 1 & 0 \end{pmatrix} \begin{pmatrix} S_{j,i} & S_{j+1,i} \\ S_{j,i+1} & S_{j+1,i+1} \end{pmatrix} \begin{pmatrix} -1 & 1 \\ 1 & 0 \end{pmatrix} \begin{pmatrix} u \\ 1 \end{pmatrix} = C \tag{2}$$

The 4 control vertices $S_{j,i}, S_{j+1,i}, S_{j,i+1}$ and $S_{j+1,i+1}$ of the B-solid for which the system (2) has a solution (u', v') so that $0 \leq u' < 1$ and $0 \leq v' < 1$, form a patch that contains the point $C(x, y, z)$. Therefore, the parameters (u_0, v_0) are: $u_0 = u' + i, v_0 = v' + j$.

Once we have obtained the (u_0, v_0, w_0), we find the coordinates (x_0, y_0, z_0) of a point C_0 in the cubic tag model,* so that: $(x_0, y_0, z_0) = \sum_{i=0}^{I} \sum_{j=0}^{J} \sum_{k=0}^{K} S_{kji} B_i(u_0) B_j(v_0) B_k(w_0)$. The (x, y, z) coordinates of a point satisfy the following expressions,

$$\begin{array}{ll} x_0 = f_1(u_0, v_0, w_0) & x = x_0 + \triangle x = f_1(u, v, w) = f_1(u_0 + \triangle u, v_0 + \triangle v, w_0 + \triangle w) \\ y_0 = f_2(u_0, v_0, w_0) & y = y_0 + \triangle y = f_2(u, v, w) = f_2(u_0 + \triangle u, v_0 + \triangle v, w_0 + \triangle w) \\ z_0 = f_3(u_0, v_0, w_0) & z = z_0 + \triangle z = f_3(u, v, w) = f_3(u_0 + \triangle u, v_0 + \triangle v, w_0 + \triangle w) \end{array} \tag{3}$$

where $f_1(u, v, w) = \sum_{i=0}^{I} \sum_{j=0}^{J} \sum_{k=0}^{K} X_{kji} B_i(u) B_j(v) B_k(w)$, $f_2(u, v, w) = \sum_{i=0}^{I} \sum_{j=0}^{J} \sum_{k=0}^{K} Y_{kji} B_i(u) B_j(v) B_k(w)$ and $f_3(u, v, w) = \sum_{i=0}^{I} \sum_{j=0}^{J} \sum_{k=0}^{K} Z_{kji} B_i(u) B_j(v) B_k(w)$. After a Taylor series expansion,

$$\begin{array}{rl} f_1(u_0 + \triangle u, v_0 + \triangle v, w_0 + \triangle w) = & f_1(u_0, v_0, w_0) + \triangle u \frac{\partial f_1}{\partial u}(u_0, v_0, w_0) + \\ \triangle v \frac{\partial f_1}{\partial v}(u_0, v_0, w_0) & + \triangle w \frac{\partial f_1}{\partial w}(u_0, v_0, w_0) + O(\triangle u) + O(\triangle v) + O(\triangle w) \\ f_2(u_0 + \triangle u, v_0 + \triangle v, w_0 + \triangle w) = & f_2(u_0, v_0, w_0) + \triangle u \frac{\partial f_2}{\partial u}(u_0, v_0, w_0) + \\ \triangle v \frac{\partial f_2}{\partial v}(u_0, v_0, w_0) & + \triangle w \frac{\partial f_2}{\partial w}(u_0, v_0, w_0) + O(\triangle u) + O(\triangle v) + O(\triangle w) \\ f_3(u_0 + \triangle u, v_0 + \triangle v, w_0 + \triangle w) = & f_3(u_0, v_0, w_0) + \triangle u \frac{\partial f_3}{\partial u}(u_0, v_0, w_0) + \\ \triangle v \frac{\partial f_3}{\partial v}(u_0, v_0, w_0) & + \triangle w \frac{\partial f_3}{\partial w}(u_0, v_0, w_0) + O(\triangle u) + O(\triangle v) + O(\triangle w) \end{array}$$

By taking derivatives of the functions, substituting their respective expressions and

*Here the blending functions are cubic according to the tag model definition

taking into account expressions from (3) we obtain,

$$\begin{aligned}
\Delta x &= x - x_0 = \Delta u \sum_{i=0}^{I}\sum_{j=0}^{J}\sum_{k=0}^{K} X_{kji} B_i'(u_0) B_j(v_0) B_k(w_0) + \\
&\Delta v \sum_{i=0}^{I}\sum_{j=0}^{J}\sum_{k=0}^{K} X_{kji} B_i(u_0) B_j'(v_0) B_k(w_0) + \Delta w \sum_{i=0}^{I}\sum_{j=0}^{J}\sum_{k=0}^{K} X_{kji} B_i(u_0) B_j(v_0) B_k'(w_0) \\
\Delta y &= y - y_0 = \Delta u \sum_{i=0}^{I}\sum_{j=0}^{J}\sum_{k=0}^{K} Y_{kji} B_i'(u_0) B_j(v_0) B_k(w_0) + \\
&\Delta v \sum_{i=0}^{I}\sum_{j=0}^{J}\sum_{k=0}^{K} Y_{kji} B_i(u_0) B_j'(v_0) B_k(w_0) + \Delta w \sum_{i=0}^{I}\sum_{j=0}^{J}\sum_{k=0}^{K} Y_{kji} B_i(u_0) B_j(v_0) B_k'(w_0) \\
\Delta z &= z - z_0 = \Delta u \sum_{i=0}^{I}\sum_{j=0}^{J}\sum_{k=0}^{K} Z_{kji} B_i'(u_0) B_j(v_0) B_k(w_0) + \\
&\Delta v \sum_{i=0}^{I}\sum_{j=0}^{J}\sum_{k=0}^{K} Z_{kji} B_i(u_0) B_j'(v_0) B_k(w_0) + \Delta w \sum_{i=0}^{I}\sum_{j=0}^{J}\sum_{k=0}^{K} Z_{kji} B_i(u_0) B_j(v_0) B_k'(w_0)
\end{aligned} \tag{4}$$

Consequently, we have three linear equations and three unknowns: $(\Delta u, \Delta v, \Delta w)$. Once we have solved the system, we obtain $\tilde{u} = \Delta u + u_0, \tilde{v} = \Delta v + v_0$ and $\tilde{w} = \Delta w + w_0$. The described procedure has an error due to the linear expansion in the Taylor formula. Hence, if the parameters $(\tilde{u}, \tilde{v}, \tilde{w})$ that are solution of (4) give a point $\tilde{C} = \sum_{i=0}^{I}\sum_{j=0}^{J}\sum_{k=0}^{K} S_{kji} B_i(\tilde{u}) B_j(\tilde{v}) B_k(\tilde{w})$ so that $||\tilde{C} - C|| > \epsilon$ for some tolerance ϵ, we update the approximations $(u_0, v_0, w_0) = (\tilde{u}, \tilde{v}, \tilde{w})$, and $(x_0, y_0, z_0) = (\tilde{x}, \tilde{y}, \tilde{z})$ and again apply the procedure until we obtain a good approximation for the point. It can be shown using the Weierstrass convergence theorem that the row of points $\{(\tilde{x}, \tilde{y}, \tilde{z})\}$ converges to the point (x, y, z). The initial parameters (u_0, v_0, w_0) are found as a linear approximation to the parameters (u, v, w) in terms of the discussed above B-spline procedure. As a consequence the initial point (x_0, y_0, z_0) lies near the point (x, y, z) and the procedure computes the parameters (u, v, w) in few iterations (empirically, we have obtained the parameters in less than 3 iterations). The procedure described here is applied to all control points of the heart model individually.

2.4 Tensor Product Representation of B-Solids

Considering the large amount of data in a 3D volume, the compact representation of a model and its computational complexity become of great importance. With this goal Guéziec in [11], working on the problem of surface reconstruction from 3D edge data, introduced surface representation with deformable splines by means of a 2D tensor product. There, a surface $Q(x, y, z) = \sum_{i=0}^{I}\sum_{j=0}^{J} S_{ji} B_i(u) B_j(v)$, in terms of a tensor product B-spline with $I \times J$ control points, is presented in a compact way: for all points of the surface, a matrix notation is employed: $Q = B_v^T S B_u$, where S is the control points matrix of dimensions $J \times I$, whose elements are the control vertices $S_{ji} \in R^3$. B_u (B_v) has dimensions $I \times I$ $(J \times J)$ gathering all spline evaluations in the blending functions $B_i(u), i = 0, ..., I$ $(B_j(v), j = 0, ..., J)$,

$$B_u = \begin{bmatrix}
B_0(u_0) & 0 & 0 & ... \\
B_1(u_0) & B_1(u_1) & 0 & ... \\
B_2(u_0) & B_2(u_1) & B_2(u_2) & ... \\
B_3(u_0) & B_3(u_1) & B_3(u_2) & ... \\
0 & B_4(u_1) & B_4(u_2) & ... \\
0 & 0 & B_5(u_2) & ... \\
. & . & . & .
\end{bmatrix} \tag{5}$$

Generalizing this notation to the solid, the control points form a three-dimensional tensor. Using square brackets to distinguish the tensor from the matrix notation, we can write: $[Q] = [S]_{kji} \otimes_i B_u \otimes_j B_v \otimes_k B_w$, where $[Q]$ is a 3D tensor of 3-vectors representing all the sampled points of the B-solid. B_u, B_v and B_w are matrices of the form in (5), corresponding to the three classes of blending functions with respect to the parameters u, v and w. $[S]_{kji} = \{S_{kji}\}_{i=0,\ldots I, j=0,\ldots J, k=0,\ldots K}$ is a 3D tensor, whose elements are the 3-vectors of control points. In particular, the elements of $[S]_{kji}$ are ordered in such a way that fixing k and j, we obtain the control points of all u iso-parametric curves, by fixing k and i we obtain the control points of the v iso-parametric curves, etc. Each matrix of the tensor $[S_{kji}]$ formed by fixing the index k contains the control points S_{kji}, belonging to the $k-$ plane (i.e. to the w iso-parametric surface of the B-spline model), and fixing the parameters j and i we obtain the $v-$ and $u-$iso-parametric planes of the B-solid, respectively.

The operation $\otimes_l$, where l denotes an index of a tensor (e.g. $l \in \{i, j, k\}$), is defined as follows, $[S]_{kji} \otimes_i B_{im} = [\sum_{i=0}^{I} S_{kji} B_{im}]_{kjm}, [S]_{kji} \otimes_j B_{jm} = [\sum_{j=0}^{J} S_{kji} B_{jm}]_{kmi}, [S]_{kji} \otimes_k B_{km} = [\sum_{k=0}^{K} S_{kji} B_{km}]_{mji}$. In other words, in order to obtain the multiplication of a tensor S by a matrix B with respect to an index l we fix an index different from l (e.g. index i) and multiply all matrices (S^i) by the matrix B. The result of multiplications between matrices (S^i) of both tensor S and the matrix B is a matrix $(S^i B)$ which is inserted in a 3D tensor, parallel to S^i. †

Because of the similarity of the multiplication of the tensor with a matrix to multiplication of matrices and for sake of simplicity we shell omit the operator $\otimes_l$ when it is clear which tensor index is fixed. In our case, we consider multiplication of the tensor by matrices B_u, B_v, B_w that act on the iso-parametric curves of the B-spline model. Given that the control points of the u iso-parametric curve can be obtained from $S_{k,j,i}$ by fixing k and j, and the v and w iso-parametric curves can be obtained by fixing k and i, and fixing j and i respectively,

$$
\begin{aligned}
[S]_{kji} B_u &= [S]_{kji} \otimes_i B_{im}(u) = [\sum_{i=0}^{I} S_{kji} B_{im}(u)]_{kjm} \\
[S]_{kji} B_v &= [S]_{kji} \otimes_j B_{jm}(v) = [\sum_{j=0}^{J} S_{kji} B_{jm}(v)]_{kmi} \\
[S]_{kji} B_w &= [S]_{kji} \otimes_k B_{km}(w) = [\sum_{k=0}^{K} S_{kji} B_{km}(w)]_{mji}
\end{aligned}
$$

3 Energy of the Deformable B-Solid

The B-solid is a deformable body with an associated energy composed of internal and external energies,

$$E_{solid} = E_{int} + E_{ext} \tag{6}$$

External forces attract the B-solid towards the tag data by minimizing its external energy E_{ext}, whereas internal forces try to preserve an ideal shape of the solid by minimizing the internal energy, E_{int}.

† For some properties of the defined operation see appendix A.

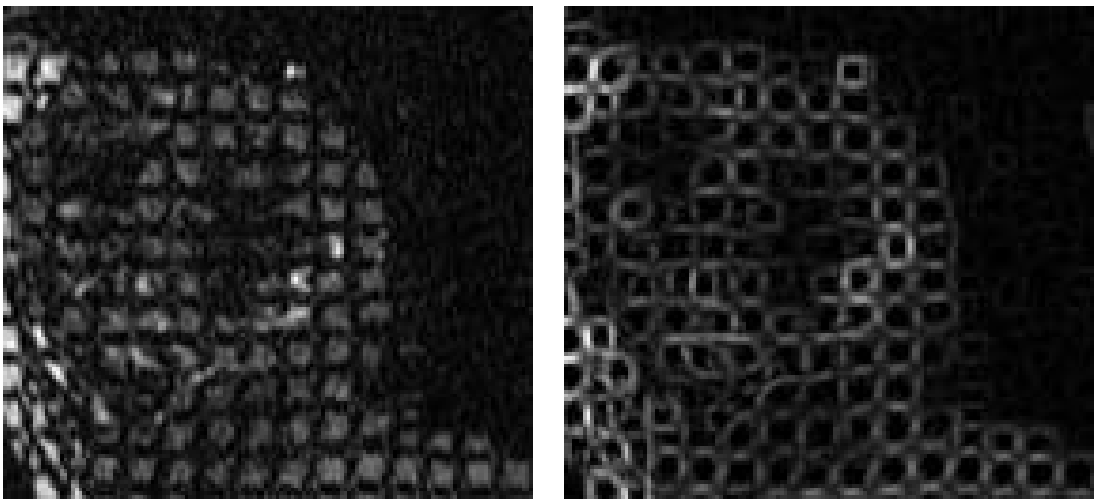

a b

Figure 7: Original tag image (a) and its map of principal curvatures (b)

3.1 Tag External Energy of the Deformable B-Solid

In this paper, we propose to detect tag lines by applying a valley detector based on Haralick's facet model [14] as a more robust and invariant technique to variations in image contrast than by searching for dark regions in the image, as previously proposed. With the facet model, a pixel neighborhood is approximated by a continuous surface. All subsequent analysis is performed on the analytical representation of the facet. By observing that locations of interest in the image are dark ridges, we create a potential field where the valleys correspond to pixels with maximal principal curvature of the intensity surface, $C_{max} = \frac{1}{2}(T_{xx} + T_{yy}) + \sqrt{(T_{xx} - T_{yy})^2 + 4T_{xy}^2}$, where T denotes the facet which approximates the surface. Computing the principal curvature of the surface, using the analytical expression from facet models is a fast approach which yields good results (see Fig. 7).

In SPAMM-images, two sets of tag lines with approximate perpendicular orientations are present. When an implicit snake is not exactly aligned with its corresponding tag line, an attraction force from tags of perpendicular orientation acts on it which may lead the snake to settle in a wrong valley. To surmount this problem, we create two directional potential fields where in each one we supress the influence of the tag lines of perpendicular orientation.

The potential field of our B-solid model is constructed as continuous surfaces derived from the image slices within which valleys correspond to the pixels with maximal principal curvatures. The principal curvature images are further filtered by a directional Gaussian (though the associated principal directions may be used to give similar results). The effect is that for the horizontal potential field, the vertical lines formed by pixels with maximal principal curvatures are smoothed and hence the effect of vertical features in horizontal potential field is diminished. An analogous situation holds for the vertical potential field. The potential energy for each point q of an implicit snake from the deformable model Q is given by its height in the potential surface P^{tag}, $E_{ext}^{tag}(q) = P^{tag}(q)$, $q \in Q$ Consequently, the closer the implicit snake is to a valley point, the lower its potential energy will be. In its attempt to minimize the potential energy, the external force pushes the implicit snake towards the local valleys of the energy landscape. In each step of the iterative procedure, the implicit snake considers a local neighborhood of its location in the potential field and

is pushed in the direction determined by the local slope of the potential field towards tag lines with similar orientation.

3.2 Contour External Energy of the Heart Model

We have adopted the strategy of combining tag and contour information with the goal of a more complete tissue deformation analysis of the heart. Without attempting to have any *a priori* point correspondences, we consider two external forces: the first external force is associated with the tag data, as we discussed in the last section, and the second is associated with the contours of the heart. Given the interdependence of both models, the heart model exerts forces on the deformable B-solid.

We construct contour potential field derived for each slice from the successive frames of images as a continuous surface, where the valleys correspond to the contours. Each pixel is assigned a value proportional to the distance to the nearest valley point from the potential surface. A fast and convenient way to construct this potential field is by distance propagation. We have used the raster scan algorithm [18] to create the map of distances. Located a model Q on the contour potential field P^{cont} the potential energy of each point q is given by its height in the contour potential field $E^{cont}_{ext}(q) = P^{cont}(q),\ q \in Q$.

3.3 Internal Energy of the Deformable B-Solid

In the classical definition of the snakes [15, 20] the internal energy is given by the membrane and thin-plate energies that are functions of the derivatives of the curve up to second order,

$$E_{int} = \tfrac{1}{2}\int \alpha||Q'(u)||^2 + \beta||Q''(u)||^2 du = \tfrac{1}{2}\sum_{j=0}^{p}\{\alpha||\sum_{i=0}^{m} S_i B_i'(u_j)||^2 + \beta||\sum_{i=0}^{m} S_i B_i''(u_j)||^2\} \qquad (7)$$

where α and β are parameters of elasticity that determine the tolerance between the different internal and external energies and $u_j, j = 0, ...m$ are the knots of the snake B-spline.

For the case of 3D deformable body, the most general case of internal energy is given by all combinations of first and second derivatives with respect to the three parameters of the B-solid: $\frac{\partial^{r+s+t}}{\partial u^r \partial v^s \partial w^t} Q(u,v,w),\ r,s,t \in \{0,1,2\}$.

Using the previously described tensor notation we define the internal energy as follows,

$$\begin{aligned} E_{int} = \ & \tfrac{1}{2}\{\sum_{r,s,t=1}^{2} \sum_{\bar{u},\bar{v},\bar{w}\in U,\ \bar{u}\neq\bar{v}\neq\bar{w}} \alpha_{\bar{u}}^{2-r}\alpha_{\bar{v}}^{2-s}\alpha_{\bar{w}}^{2-t}\beta_{\bar{u}}^{r-1}\beta_{\bar{v}}^{s-1}\beta_{\bar{w}}^{t-1}||SB_{\bar{u}}^{(r)}B_{\bar{v}}^{(s)}B_{\bar{w}}^{(t)}||^2 + \\ & \sum_{r,s=1}^{2} \sum_{\bar{u},\bar{v}\in U,\ \bar{u}\neq\bar{v}} \alpha_{\bar{u}}^{2-r}\alpha_{\bar{v}}^{2-s}\beta_{\bar{u}}^{r-1}\beta_{\bar{v}}^{s-1}||SB_{\bar{u}}^{(r)}B_{\bar{v}}^{(s)}||^2 + \sum_{r=1}^{2}\sum_{\bar{u}\in U}\alpha_{\bar{u}}^{2-r}\beta_{\bar{u}}^{r-1}||SB_{\bar{u}}^{(r)}||^2\} \end{aligned} \qquad (8)$$

where superscripts in parantheses denote derivatives U is the set of parameters $\{u,v,w\}$ and $B_{\bar{u}}^{(r)}, B_{\bar{u}}^{(s)}, ...$ are matrices formed by the $r,s,t-$derivatives of the blending functions with respect to the parameter $\bar{u}$ as shown in (5). Note that the notation: $\sum_{r=1}^{2}\sum_{\bar{u}\in U} ...B_{\bar{u}}^{(r)}$ in fact expresses all first and second derivatives of blending functions with respect to each parameter (u,v,w). Analogously, in the first and second term the parameter $\bar{u}$ denotes certain parameter of U[‡]. In (8), the first summand measures the internal energy on all solid cubes of the deformable body, whereas the other terms measure terms of the internal energy of all iso-parametric surfaces and curves.

[‡]By $\bar{u}$, we mean the actual parameter, as opposed to a specific parameter value.

The internal energy defined in terms of derivatives up to second order takes charge of deforming the B-solid (iso-parametric curves, surfaces or solid patches) so that it preserves its continuous and smooth shape. However, minimizing the derivatives result in undesired shrinking effects. To avoid this problem, some authors minimize the difference in the membrane and thin-plate energies for the snake from an ideal model [31, 29]. This approach has demonstrated good results in some applications, but it does not restrict the deformation with respect to a model. Considering an iterative procedure for energy-minimization, the difference between the body shapes in sequential steps can be quite large. In our case, we consider an approximate rectangular solid. We are interested in small deformations of our three dimensional solid using as a reference an ideal rectangular three dimensional model. We modify the internal energy so that it measures the distance between the deformable body and a model. Therefore, this internal energy is an analog of internal energy of 1D deformable models considered in [31, 29]. Let $Q(x,y,z) = \sum_{i=0}^{I}\sum_{j=0}^{J}\sum_{k=0}^{K} S^0_{kji} B_u(u) B_v(v) B_w(w)$ be such a model. The modified internal energy has the following form,

$$E_{int} = \frac{1}{2}\{ \sum_{r,s,t=1}^{2} \sum_{\bar{u},\bar{v},\bar{w}\in U,\ \bar{u}\neq\bar{v}\neq\bar{w}} \alpha_{\bar{u}}^{2-r}\alpha_{\bar{v}}^{2-s}\alpha_{\bar{w}}^{2-t}\beta_{\bar{u}}^{r-1}\beta_{\bar{v}}^{s-1}\beta_{\bar{w}}^{t-1} ||SB_{\bar{u}}^{(r)}B_{\bar{v}}^{(s)}B_{\bar{w}}^{(t)} - S^0 B_{\bar{u}}^{(r)}B_{\bar{v}}^{(s)}B_{\bar{w}}^{(t)}||^2 +$$
$$\sum_{r,s=1}^{2} \sum_{\bar{u},\bar{v}\in U,\ \bar{u}\neq\bar{v}} \alpha_{\bar{u}}^{2-r}\alpha_{\bar{v}}^{2-s}\beta_{\bar{u}}^{r-1}\beta_{\bar{v}}^{s-1} ||SB_{\bar{u}}^{(r)}B_{\bar{v}}^{(s)} - S^0 B_{\bar{u}}^{(r)}B_{\bar{v}}^{(s)}||^2 + \sum_{r=1}^{2}\sum_{\bar{u}\in U} \alpha_{\bar{u}}^{2-r}\beta_{\bar{u}}^{r-1} ||SB_{\bar{u}}^{(r)} - S^0 B_{\bar{u}}^{(r)}||^2 \}$$

Using the distributive property of tensor multiplications defined in appendix A, we obtain,

$$E_{int} = \frac{1}{2}\{ \sum_{r,s,t=1}^{2} \sum_{\bar{u},\bar{v},\bar{w}\in U,\ \bar{u}\neq\bar{v}\neq\bar{w}} \alpha_{\bar{u}}^{2-r}\alpha_{\bar{v}}^{2-s}\alpha_{\bar{w}}^{2-t}\beta_{\bar{u}}^{r-1}\beta_{\bar{v}}^{s-1}\beta_{\bar{w}}^{t-1} ||(S - S^0)B_{\bar{u}}^{(r)}B_{\bar{v}}^{(s)}B_{\bar{w}}^{(t)}||^2 +$$
$$\sum_{r,s=1}^{2} \sum_{\bar{u},\bar{v}\in U,\ \bar{u}\neq\bar{v}} \alpha_{\bar{u}}^{2-r}\alpha_{\bar{v}}^{2-s}\beta_{\bar{u}}^{r-1}\beta_{\bar{v}}^{s-1} ||(S - S^0)B_{\bar{u}}^{(r)}B_{\bar{v}}^{(s)}||^2 + \sum_{r=1}^{2}\sum_{\bar{u}\in U} \alpha_{\bar{u}}^{2-r}\beta_{\bar{u}}^{r-1} ||(S - S^0)B_{\bar{u}}^{(r)}||^2 \}$$

Some nice properties of the modified internal energy in relation with the energy minimizing procedure will be described in subsequent sections.

4 Non-Rigid Registration of B-Solid to Tag Data

The problem of localization of tag data by a B-solid is an energy-minimizing problem. The B-solid is placed around the data and is deformed, i.e., its iso-parametric surfaces are deformed in order to minimize its energy. The local minimum of the energy that is found in the images from the first temporal frame corresponds to the solution of the localization problem. The resulting B-solid from each frame is then used as the initial solid in order to track the deformation in the next volumetric image frame.

4.1 Initialization of the B-Solid

For the purpose of initialization in the first volumetric frame, a control polygon method was previously defined in [7] and later used in [20, 10] for curve matching. This method is easily extendable for initializing the B-solid. This technique however is known to have numerical stability problems [11]. Hence, we consider an alternate approach to B-solid initialization, where we do not put strong constraints on necessarily good approximation of the data by the initial position of the control vertices. Instead, we consider appropriate internal forces that cope with the inexact initial positions of the deformable B-solid. In this case, the user only delimits the region of interest in one or each slices of images

from the initial temporal frame and gives the initial distance between the u and v iso-parametric planes. The distance between the w-iso-parametric planes is determined by the slice separation in volumetric short-axis SPAMM images. The initial B-solid is defined as the minimum three-dimensional rectangular grid which contains the region(s) of interest. Since the internal force takes charge of local displacements [29], rotation and displacement of the implicit snakes between subsequent images is usually limited to half of the tag line interdistances. An example of an intersection on an initial B-solid can be seen in Fig. 8 (a).

4.2 Energy-Minimization Procedure

Let us consider equation (6). We are looking for a solid S that gives a minimum of the energy, E_{solid}, a linear combination of internal energy and tag external energy,

$$\frac{\partial E_{solid}(Q)}{\partial S} = \frac{\partial E_{int}(Q)}{\partial S} + \frac{\partial E_{ext}^{tag}(Q)}{\partial S} = 0 \tag{9}$$

A solution can be viewed as one which achieves an equilibrium among the internal and external forces in the energy equation and reaches a minimum of the total energy. The solid body is under the control of internal forces that impose regularity on the B-solid, whereas the external forces attract the B-solid towards the data. Usually, the energy is not convex, and in general, it is better to have methods which find global minima no matter what the energy field. However, finding a global minimum of the considered problem is too complicated to be treatable for the B-solid. Therefore, we look for a solution that gives a good local minimum of the energy. There may be many local minima of E. Thus, it is important to define the external and internal forces, reflecting the need for tag localization as well as boundary tracking so that the found solution is a good solution for the localization problem.

To provide dynamics for the deformable body, the associated evolution equation is considered,

$$-\frac{\partial S}{\partial t} = \frac{\partial E_{int}(Q)}{\partial S} + \frac{\partial E_{ext}^{tag}(Q)}{\partial S} \tag{10}$$

A solution to the static problem (9) is achieved when the solution $S(t)$ stabilizes [8].

Taking the derivative of the internal energy in (8) and substituting $A_{\bar{u}}^{(r)} = B_{\bar{u}}^{(r)}\ B_{\bar{u}}^{(r)T}$, $A_{\bar{v}}^{(r)T} = B_{\bar{v}}^{(r)}\ B_{\bar{v}}^{(r)T}$, ..., we obtain,

$$\begin{aligned}\frac{\partial E_{int}(Q)}{\partial S} &= \sum_{r,s,t=1}^{2} \sum_{\bar{u},\bar{v},\bar{w}\in U,\ \bar{u}\neq\bar{v}\neq\bar{w}} \alpha_{\bar{u}}^{2-r}\alpha_{\bar{v}}^{2-s}\alpha_{\bar{w}}^{2-t}\beta_{\bar{u}}^{r-1}\beta_{\bar{v}}^{s-1}\beta_{\bar{w}}^{t-1}(S-S^0)A_{\bar{u}}^{(r)}A_{\bar{v}}^{(s)}A_{\bar{w}}^{(t)} \\ &\sum_{r,s=1}^{2} \sum_{\bar{u},\bar{v}\in U,\ \bar{u}\neq\bar{v}} \alpha_{\bar{u}}^{2-r}\alpha_{\bar{v}}^{2-s}\beta_{\bar{v}}^{r-1}\beta_{\bar{v}}^{s-1}(S-S^0)A_{\bar{u}}^{(r)}A_{\bar{v}}^{(s)} + \sum_{r=1}^{2} \sum_{\bar{u}\in U} \alpha_{\bar{u}}^{2-r}\beta_{\bar{u}}^{r-1}(S-S^0)A_{\bar{u}}^{(r)}\end{aligned}$$

And, writing the sums in matrix form, we obtain,

$$\begin{aligned}\frac{\partial E_{int}(Q)}{\partial S} &= (S-S^0)((\alpha_u A'_u + \beta_u A''_u)(\alpha_v A'_v + \beta_v A''_v)(\alpha_w A'_w + \beta_w A''_w) + \\ &(\alpha_u A'_u + \beta_u A''_u)(\alpha_v A'_v + \beta_v A''_v) + (\alpha_u A'_u + \beta_u A''_u)(\alpha_w A'_w + \beta_w A''_w) + \\ &(\alpha_v A'_v + \beta_v A''_v)(\alpha_w A'_w + \beta_w A''_w) + (\alpha_u A'_u + \beta_u A''_u) + (\alpha_v A'_v + \beta_v A''_v) + (\alpha_w A'_w + \beta_w A''_w))\end{aligned}$$

Let $K_u = \alpha_u A'_u + \beta_u A''_u$, $K_v = \alpha_v A'_v + \beta_v A''_v$, and $K_w = \alpha_w A'_w + \beta_w A''_w$. Then,

$$\frac{\partial E_{int}(Q)}{\partial S} = (S-S^0)(K_u K_v K_w + K_u K_v + K_u K_w + K_v K_w + K_u + K_v + K_w)$$

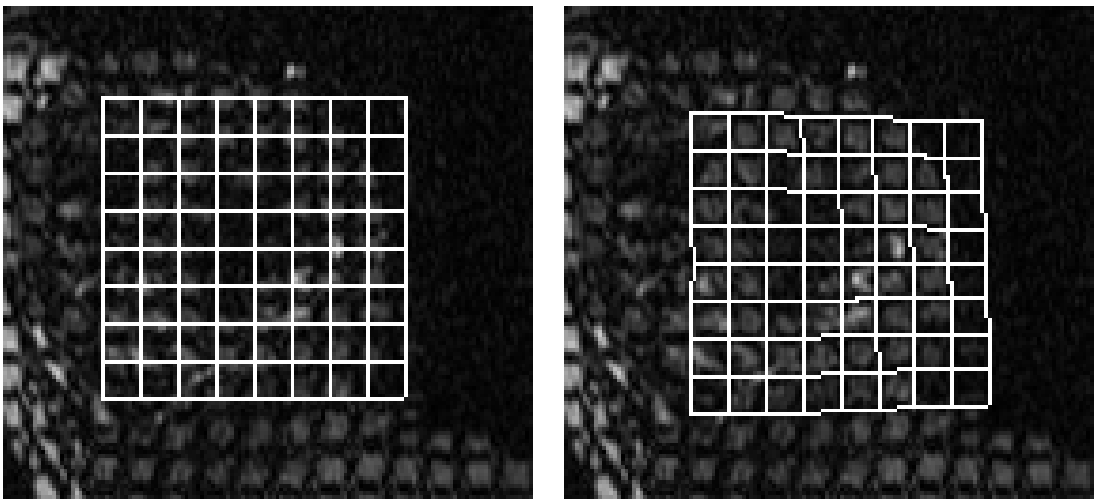

a b

Figure 8: Intersections of the initial B-solid and its deformation after tags localization

Taking derivative of external energy with respect to the control points,

$$\frac{\partial E_{ext}^{tag}(Q)}{\partial S} = \bigtriangledown P^{tag}(Q)\frac{\partial Q}{\partial S} = F^{tag}(Q)\frac{\partial (SB_uB_vB_w)}{\partial S} = F^{tag}(Q)B_uB_vB_w$$

where $F^{tag} = \bigtriangledown P^{tag}$ denotes the external force of the deformable B-solid derived from the tag data (as before tag is for tag).

After formulating the semi-explicit evolution equation using finite differences with time step γ and substituting in equation (10), we obtain,

$$\begin{aligned} -\gamma\frac{\partial S}{\partial t} &= \frac{\partial E_{int}(Q^{k+1})}{\partial S} + \frac{\partial E_{ext}^{tag}(Q^k)}{\partial S} \\ -\gamma(S^{k+1} - S^k) &= (S^{k+1} - S^0)(K_uK_vK_w + K_uK_v + K_uK_w + K_vK_w + K_u + K_v + K_w) \\ &\quad + F^{tag}(Q^k(u,v,w))B_uB_vB_w \end{aligned}$$

The parameter γ is called the damping parameter. It determines the velocity of the moving pixels of the body. Given γ close to unity leads to an acceptable velocity for the iso-parametric curves (a fact we have confirmed empirically). We reduce the expression to the following linear system,

$$S^{k+1} = (S^k + F_{init}(S^0) - F^{tag}(Q)B_uB_vB_w)(K_u + I)^{-1}(K_v + I)^{-1}(K_w + I)^{-1} \quad (11)$$

where $F_{init}(S^0) = S^0(K_u+I)(K_v+I)(K_w+I) - S^0$ and I denotes the identity matrix. F_{init} can be thought of as a force that always tries to push the deformable body towards the model S^0. The combination of both forces (the external force that attracts the body to the image data and the F_{init} force preserving the similarity to an initial model) allows for some displacement for the deformable body and thus less dependence on initial position. A nice property of the internal force preserving a predetermined model is that it does not change the numerical stability of the linear system (11), nor significantly increases the computational complexity of the method. This is due to the fact that this force consists of adding a temporally constant tensor which depends on the model and the stiffness matrices K_u, K_v and K_w. In Fig. 8 (b) a result of the localization procedure can be seen.

The linear system (11) contains three independent linear equations for (X, Y, Z) coordinates of the control vertices. Similar to the case of 1D and 2D deformable models, the three stiffness matrices regarding the three parameters $(K_u+\gamma I), (K_v+\gamma I)$ and $(K_w+\gamma I)$ are diagonal, symmetric, and positive definite. Given that the parameters of elasticity are

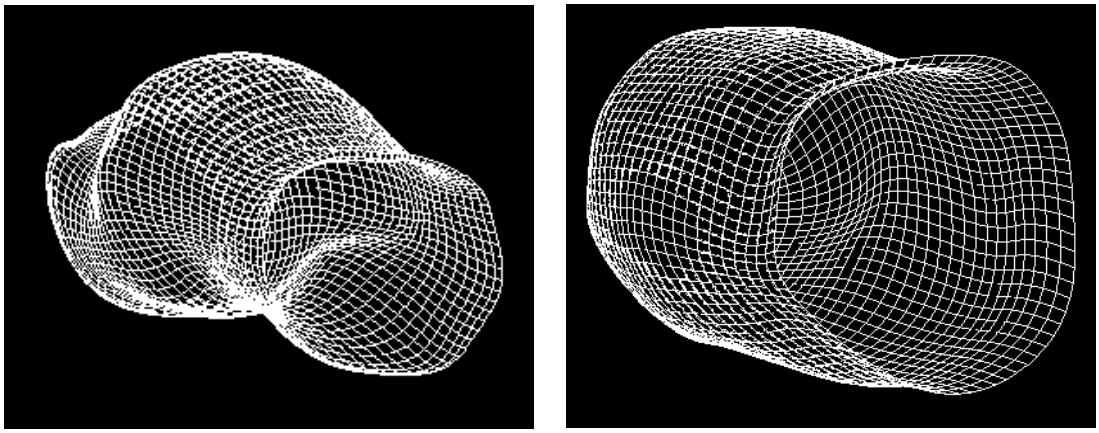

a b

Figure 9: Approximation to endocardium and epicardium by B-splines

constant over time, the factorization of the matrices is done only once at the beginning. This in fact, is very important for handling the 3D model fitting to the 3D data, as well as for speeding up the computational process.

The linear system in (11) is a 3D analog of the snake computational scheme. In the same way the deformation of the body can be considered as a composition of body attraction towards the data followed by smoothing action in accordance with the constraints imposed by the internal energy. It is worthwhile to emphasize that the smoothing operator is presented by decoupled operators with respect to the parameters. Thus, the smoothing effect of each of them can be estimated. In addition, due to the fact that the smoothing matrices correspond to differential operators with respect to different parameters, the order of applying them is unimportant (see Appendix A).

5 B-Spline Approximation to Endocardium and Epicardium

The problem of localization of the heart is considered here in order to construct a heart model using the endocardial and epicardial contours in image slices in the first temporal volumetric frame. For this purpose we need approximations to endocardium and epicardium of the heart by B-spline surfaces. To fit the complexity of the heart shape we have used a cubic-quadric partially closed surface with six slices of control points and sixteen control points in each slice. We assume the heart ventricle contour points are first determined by a low-level process from tagged images or are specified on the images by the user. A potential function is defined as the distance from each B-spline surface point to the nearest contour point, and the surface model is optimized by conjugate gradient descent. This potential tolerates large deviations of the initial model to the object because even when there are some false contour points. Attention was also paid to the smoothness of the surface in this case. Smoothness was enforced by applying second order derivative penalties at all points along the surface. The heart boundaries approximation allows us to construct the heart model expressed by means of the control points of the B-spline surfaces. The surfaces are then used to create the heart model. In Fig. 9 both surfaces constructed from contours of Fig. 4 can be seen.

6 Tracking of Heart Motion by Deformable Solid

The tracking procedure is analogous to the localization procedure of the deformable B-solid with the only difference that tag and heart models contribute to the energy of the B-solid.

6.1 Integrated Tag Grid and Heart Boundaries Tracking

Both the tag and the heart models are interdependent since they are part of the same tissue. Hence, the energy minimization is done affecting only the B-solid model. An explicit expression of the dependence of the tag model on the heart model is necessary.

Given the tag model located on the tag potential field and the heart model on the potential field derived from the heart boundaries, we look for control points of the B-solid that minimize both external energies. This leads us to consider the derivative of both external energies with respect to the control vertices of the B-solid.

Since the potential field is constructed by distance propagation from the heart contours, the external energy concerning the contour information is given by

$$E_{ext}^{cont} = ||S/_H(x,y,z) - C(x,y,z)||^2 = \sum_{r=0}^{R}\sum_{s=0}^{S}\sum_{t=0}^{T}||\sum_{o=0}^{O}\sum_{p=0}^{P}\sum_{q=0}^{Q} H_{qpo}B_o(\bar{u}_r)B_p(\bar{v}_s)B_q(\bar{w}_t) - C(x,y,z)||^2$$

where H_{qpo} denotes the control vertices of number $O \times P \times Q$ of the heart boundaries B-spline representation and $(\bar{u}_r, \bar{v}_s, \bar{w}_t), r = 0, ..., R,\ s = 0, ..., S,\ t = 0, ..., T$ are the knots. As a note, since we only have endocardial and epicardial surfaces available, $P = S = 1$ in the above expression, furthermore B_p is linear.

In the energy-minimizing procedure we look for a B-solid determined by its control vertices that minimizes both external and internal energies. After taking the derivative of the contour external energy with respect to the control vertices of the B-solid, we obtain,

$$\frac{\partial E_{ext}^{cont}}{\partial S_{kji}} = 2\sum_{o=0}^{O}\sum_{p=0}^{P}\sum_{q=0}^{Q} d_c \frac{\partial (S/_H)}{\partial H_{qpo}}\frac{\partial H_{qpo}}{\partial S_{kji}} = 2\sum_{o=0}^{O}\sum_{p=0}^{P}\sum_{q=0}^{Q}\sum_{r=0}^{R}\sum_{s=0}^{S}\sum_{t=0}^{T} d_c B_o(\bar{u}_r)B_p(\bar{v}_s)B_q(\bar{w}_t)\frac{\partial H_{qpo}}{\partial S_{kji}}$$

where $d_c = \sum_{l=0}^{O}\sum_{m=0}^{P}\sum_{n=0}^{Q}||H_{nml}B_l(\bar{u}_r)B_m(\bar{v}_s)B_n(\bar{w}_t) - C(x,y,z)||$. This distance is provided by the contour potential field.

Let the point $H_{qpo}(x,y,z)$ be represented in the deformable B-solid as $H_{qpo} = \sum_{i=0}^{I}\sum_{j=0}^{J}\sum_{k=0}^{K} S_{kji}B_i(u_0)B_j(v_0)B_k(w_0)$. The parameters (u_0, v_0, w_0) exist because the model is a B-solid body containing the heart (i.e. the regions of interest defined by the endocardial and epicardial contours in all slices). Therefore, it follows that: $\frac{\partial H_{qpo}}{\partial S_{kji}} = B_i(u_0)B_j(v_0)B_k(w_0)$.

In order to find the parameters (u_0, v_0, w_0) which give the relation between the control vertex of the heart model and the coordinate system of the tag model we apply the procedure that defines the relation between the tag model and heart representation of section 2.3.

As a result we get the following expression for the derivative of the external energy that determines the contour external force for each control vertex of the control point S_{kji} of the B-solid, $F_{kji}^{cont} = \frac{\partial E_{ext}^{cont}}{\partial S_{kji}} = 2\sum_{o=0}^{O}\sum_{p=0}^{P}\sum_{q=0}^{Q}\sum_{r=0}^{R}\sum_{s=0}^{S}\sum_{t=0}^{T} d_c B_o(\bar{u}_r)B_p(\bar{v}_s)B_q(\bar{w}_t)B_i(u_0)B_j(v_0)B_k(w_0)$.

The tracking problem is an energy minimizing process where the energy of the B-solid is defined by its internal, tag external and contour external energies,

$$E_{solid} = E_{int} + E_{ext}^{tag} + E_{ext}^{cont}$$

Following the same energy-minimization procedure as in the tracking problem, we obtain the following iterative procedure for integrated tracking of tag and contour data,

$$S^{k+1} = (S^k + F_{init}(S^0) - F^{tag}(Q)B_uB_vB_w - F^{cont}(Q))(K_u + I)^{-1}(K_v + I)^{-1}(K_w + I)^{-1} \quad (12)$$

In the above equation, *tag* denotes tag, and *cont* denotes contour energies.

In Fig. 10 an example of two frames considered in the tracking process is shown. At the base of the heart the grid (that corresponds to a w iso-parametric surface of the B-solid) is almost not deformed because the external force is applied only to the heart tissue which consists of a small area in the base of the heart. A small twisting deformation is possible to estimate in the images from the second column. In Fig. 10 (d) and (e) a slice of the heart located in the B-solid can be seen in the two consequetive frames. The deformation of the heart can be estimated in the Fig. 10 (f).

Note that in this case no correspondence of points between nodes of the model and tag intersections is necessary. In addition, the interpolation of forces to nodes of the model is implicit. Also, as the three-dimensional motion is captured no check is necessary in each step to confirm that considered tag data lie inside the myocardial contours as done in [35].

6.2 Numerical Complexity

In the usual way of treating this problem (i.e. 2D deformable body) [31] the data are presented in a vector and thus the resulting linear systems (11) and (12) are of size $((IJK) \times (IJK))$. In addition, in this case the matrices are sparse and not diagonal [35, 31]. This is in contrast with the case of 1D deformable models (snakes). This additionally complicates the computational burden. In the case of B-solid from (11) and (12), it can be seen that the numerical complexity of each iteration of the energy-mimizing procedure is $O(I \times J \times K)$. This fact is very important so as to make the procedure practical and in dealing with real three-dimensional image analysis problems.

7 Extension of the Approach to the Analysis of SA and LA Images

In this work we have only considered short axes images (SA). Since the external forces applied to the implicit snakes belong to the imaging planes, the deformation of the B-solid caused by the tag and contour data is mainly in the plane $(x-y)$. The internal forces are three-dimensional however and, can in fact change the z coordinate of the B-solid points. But this is not sufficient to provide out-of-plane movement of the material points of the heart. To solve this problem, authors have considered images of short and long axes views consisting of two mutually orthogonal sets of images.

The approach of localizing and tracking of tag and contour data by B-solid is extendable to analysis of information from SA and LA images. We describe here how to obtain three-dimensional tissue movement by treating SA images with two-dimensional tags and LA images with one-dimensional tags; i.e., we assume that in the SA views there are two sets of horizontal tag planes, whereas in the LA images there is only one set of tagging planes. Let us consider SA view images where at the initial moment the imaging planes are parallel to the $(x-y)$ plane. From the fact that tagging planes are orthogonal to the imaging planes, it follows that the tagging planes are parallel to the planes $(x-z)$ and $(y-z)$. Without loss of generality, we can consider that in the LA view the imaging planes

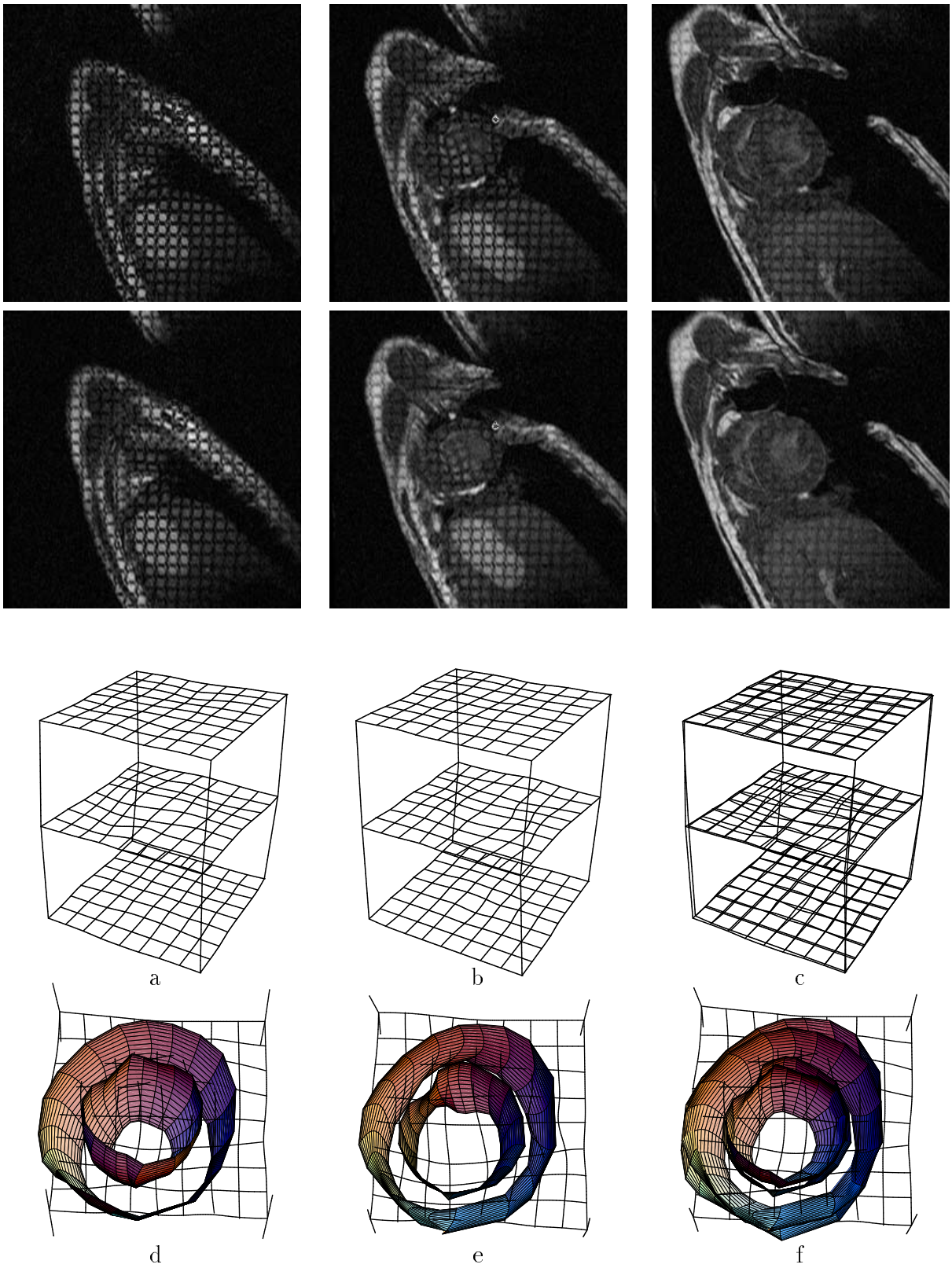

Figure 10: Tracking of deformation: different slices of images from two consequetive frames given in the first ans second row, respectively, and the corresponding B-solids (a) and (b). The deformation can be estimated in the superposition of both B-solids given in (c). Slices of heart boundaries located into the B-solid in two consequetive frames are given in (d) and (e) and their comparison can be seen in (f)

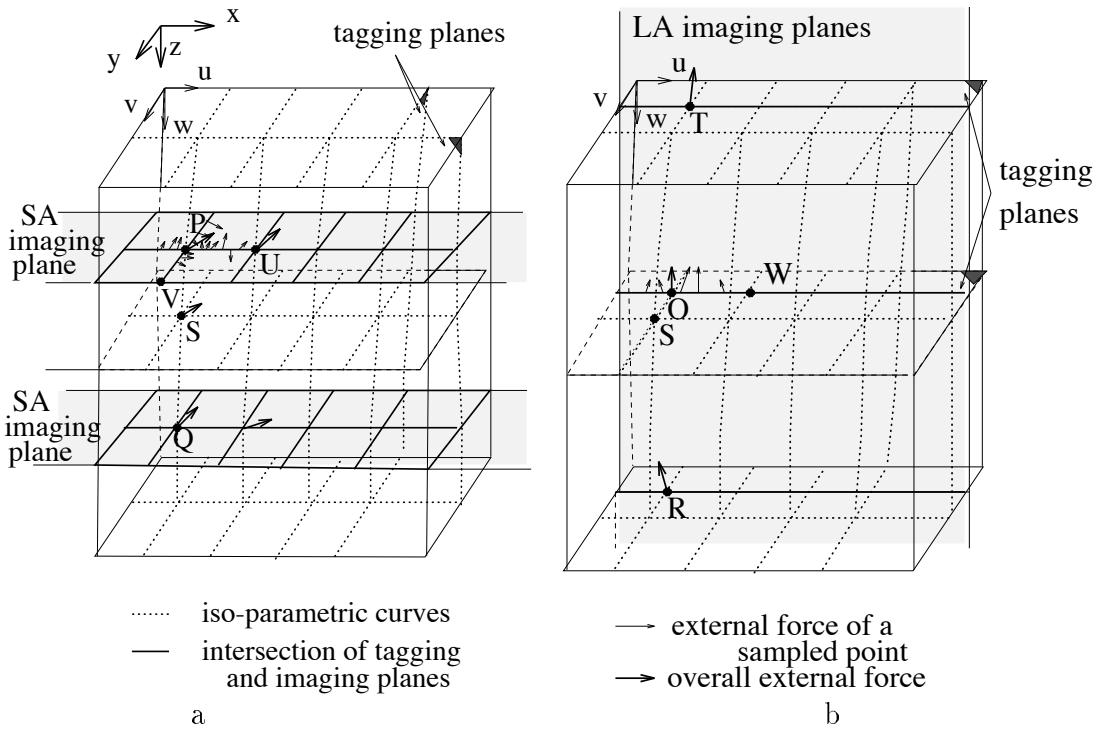

Figure 11: Intersection of a B-solid with SA view images (a) and LA view images (b)

are parallel to the plane $(x-z)$ and the tagging planes are parallel to the planes $(x-y)$ (see Fig. 11). Since a main source of information about the tissue movement is given by the deformation of the tag planes, we define the B-solid so that the iso-parametric planes correspond to the tagging planes. In particular, u and v iso-parametric planes are aligned with tag planes from the SA images and w iso-parametric planes are aligned with the tag planes from the LA images. As a consequence, the iso-parametric curves, determined by the intersections of the iso-parametric planes, correspond to the intersections of the tagging planes.

By definition the external forces of the B-solid are applied to the control vertices. The external forces of the B-solid are obtained by running patches on the iso-parametric curve and assigning the overall external force to the control vertices. In the case of B-solids constructed by SA view images, the u and v iso-parametric curves belong to the imaging planes. Since the potential field is constructed by considering the features (principal curvatures) of the imaging planes, the external forces are defined for each point of the imaging plane, in particular for the points of the iso-parametric curves.

In case of B-solid constructed by SA and LA view images, the iso-parametric curves do not belong to the imaging planes. They intersect the imaging planes and thus, only isolated points are attracted by external forces from the imaging planes (e.g. points P and Q in Fig. 11 (a) and point O in Fig. 11 (b)). Considering only the external force on these points would mean to consider only isolated tag data and not tag lines. Instead, we use the fact that the iso-parametric curves (e.g. the curve SP) intersect the imaging planes in tag lines (e.g. curves PU and PV). We estimate the external force to the control points considering the tag lines analogously to the case of implicit snakes in B-solid constructed from SA images (see Appendix B). Once we have determined the external forces of points on the iso-parametric curves of the B-solid, we apply the energy-minimization procedure to localize the tag and contour data and track the heart motion.

8 Conclusions

In conclusion, a novel three-dimensional B-spline deformable model is proposed for locating, and tracking the heart's deformation in a time sequence of 3D volumetric SPAMM images with implicit snakes. B-spline bases provide local control of shape, compact representation, and parametric smoothness. The B-solid proposed in the paper deforms in space, adjusting to tag and contour data from different slices reflecting the continuity and smoothness of the three-dimensional tissue deformations. As a consequence of the approach, localization, displacement fitting and interpolation of tag and contour information are performed in a single procedure. A heart volumetric model was also constructed as a tensor product of three-dimensional B-splines in order to incorporate data from endocardial and epicardial B-spline surfaces of the left ventricle. The heart model approximates the epicardium and endocardium and restricts the deformation analysis to the heart tissue.

In applying the B-solid to tagged images, information from data in different slices are used, making the approach robust and precise against noise. Although the deformable B-solid presented here was created from tensor product of non-periodic B-splines in the cartesian coordinate frame, this need not be the case. It is possible for example, to create B-solids adaptable to analysis of star-burst tagged MR images.

The B-solid considered here detects local deformations of the heart and allows local measurements of important cardiac function characteristics. Our future work includes extraction of 3D motion of heart's material points with B-solids, and estimation of functional characteristics of the cardiac muscle from our analysis of SA and LA images.

Acknowledgements

This work has been supported by a grant TIC91-0430 from the Spanish Ministry of Education and Science and grants from National Science Foundation and The Whitaker Biomedical Engineering Foundation.

Appendix A: Properties of Three-Dimensional Tensors

In accordance with the definition of the operation $\otimes_l$ defined in section 2.4 to obtain the expression $[S_{kji}] \otimes_l B$ we fix an index different from l (e.g. the index i) and multiply all the resulting matrices (S^i) by the matrix B. The result of the multiplications between matrices (S^i) of both tensors and the matrix B is a matrix (S^iB) forming part of the resulting tensor $([S^iB]_i)$. It is easy to show that the same result is obtained if we fix the other index different from l and carry out multiplications. For example, given $l = k$ and fixing indices i and j, we obtain the same expression,

$$[S]_{ijk} \otimes_k B_{kp}(u) = [S^iB]_i = [[\sum_{k=0}^{K} S_{ijk}B_{kp}]_{jp}]_i = [\sum_{k=0}^{K} S_{ijk}B_{kp}]_{ijp}$$
$$[S]_{ijk} \otimes_k B_{kp}(u) = [S^jB]_j = [[\sum_{k=0}^{K} S_{ijk}B_{kp}]_{ip}]_j = [\sum_{k=0}^{K} S_{ijk}B_{kp}]_{ijp}$$

From the definition of the operator $\otimes$, it follows that the operator is linear,

$$[S]_{kji} \otimes_l (cB) = c[S]_{kji} \otimes_l B \text{ and } ([S]_{kji} \otimes_l (B_1 \oplus B_2) = ([S]_{kji} \otimes_l B_1) \oplus ([S]_{kji} \otimes_l B_2),$$

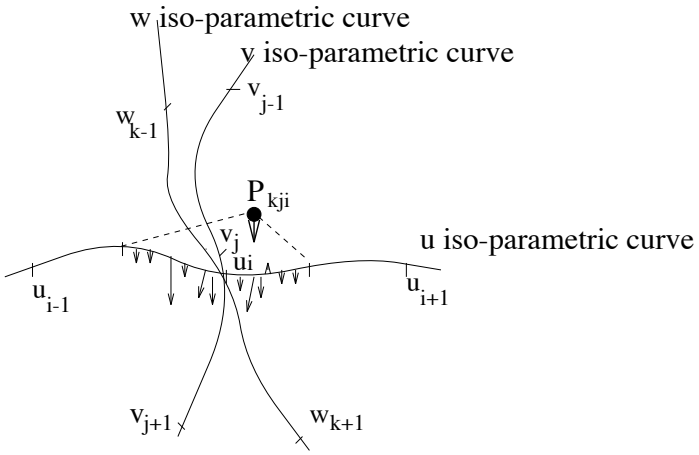

Figure 12: External force of a control vertex assigned from the external forces of sampled points of u iso-parametric curve

where $l \in \{i, j, k\}$. The linearity property of the operator $\otimes$ assures that the product is a tensor [30]. The operators $\oplus$ and $\ominus$ (see bellow) are the elementwise sum and subtraction of two tensors. Besides the linearity, the multiplication satisfies the following associative, distributive and commutative properties,

$$([S]_{kji} \oplus [T]_{kji}) \otimes_m B = ([S]_{kji} \otimes_m B) \oplus ([T]_{kji} \otimes_m B)$$
$$([S]_{kji} \ominus [T]_{kji}) \otimes_m B = ([S]_{kji} \otimes_m B) \ominus ([T]_{kji} \otimes_m B)$$
$$([S]_{kji} \otimes_l B_1) \otimes_m B_2 = ([S]_{kji} \otimes_m B_2) \otimes_l B_1, \text{ where } m, l \in \{i, j, k\}$$

Obviously, the condition for these operations is that both tensors are of the same size. As before, note that in the expression $m, l \in \{i, j, k\}$, m and l denote a certain index and not its value.

Immediately from the definition it follows that in case of multiplication of 2D tensor with a matrix it becomes a standart multiplication of matrices.

Appendix B: Determining External Energy and Forces on Control Vertices

By translating the control vertices of the B-solid the model deforms locally and in so doing decreases its external energy. The external energy of a control vertex should summarize the external energies of sampled points of the model that depend on the control vertex.

Let us consider the external force of a control point P_{kji} (see Fig. 12) from the B-solid [§]. By definition, each control vertex of the B-solid affects three iso-parametric curves corresponding to the three parameters (u, v, w). For each iso-parametric curve there are few patches that are determined by the control vertex P_{kji}. The external energy (and force, respectively) of the control vertex is determined as the overall energy (and force) of the sampled pixels from these patches.

Let us consider the u iso-parametric curve $Q(u) = \sum_{i=0}^{I} \sum_{j=0}^{J} \sum_{k=0}^{K} S_{kji} B(u) B(v_j) B(w_k)$ obtained by fixing the parameters $v = v_j$ and $w = w_k$ in the B-solid representation. From the properties of the B-splines, it follows that $Q(u) = \sum_{i=0}^{I} S_{kji} B(u)$. Since the B-solid is

[§] For the control vertices of the heart model, the procedure is analogous

constructed by cubic splines, for the curve Q the following formulas are valid [22],

$$Q(u_r) = \frac{1}{6}(P_{kj(r-1)} + 4P_{kjr} + P_{kj(r+1)}) \text{ for } r = i-1, i, i+1 \quad (13)$$

where u_{i-1}, u_i, u_{i+1} are the knots of the splines, and $P_{kji-2}, P_{kji-1}, P_{kji}, P_{kji+1}, P_{kji+2}$ are control vertices. Let $Q_r, r = i-1, i, i+1$ denotes the r-th patch of the B-spline curve that is the patch of the curve delimited by the sampled points $Q(u_r)$ and $Q(u_{r+1})$. Because of the local property of B-splines, the control vertex P_{kji} affects only patches Q_{i-1}, Q_i and Q_{i+1}. It is easy to see in (13) that moving the control vertex P_i the most affected sampled points from the curve is the point $Q(u_i)$.

A way to estimate the external force of control vertex, P_{kji} is by taking the mean value of the external forces of sampled points from the three patches with a weight proportional to the distance to point, $Q(u_i)$. Considering three patches, the process of estimating the external force leads to averaging the external energy along large part of the curve. As a consequence, local deformation of tag lines can not be captured. Hence, we consider a part of the curve with a length approximately equal to the average distance among tag lines (i.e. equal to a patch of the curve) and estimate the external energy of the control vertex as the average value of the energies of sampled points located in this part of the curve. Taking into account the equal influence of control vertex P_{kji} on patches Q_{i-1} and Q_i, the external energy is given by a normalized sum of the external energies of sampled points belonging to the second half of patch Q_{i-1} and first half of patch Q_i,

$$E_{ext}(P_{kji}) = \frac{1}{L}\sum_{l=0}^{L-1} E_{ext}(Q(\frac{u_i + u_{i-1}}{2} + l \ \ step_u))$$

where $step_u = \frac{1}{L}(\frac{u_{i+1}+u_i}{2} - \frac{u_i+u_{i-1}}{2}) = \frac{u_{i+1}-u_{i-1}}{2L}$ and L must be large enough to assure that the sampled points are neighbor pixels in the potential field (we have used $L = 20$).

As defined above, the external energy of each sampled point from the B-solid is a function of its height in the potential field. The external force of a sampled point located in the potential field is given by the gradient of the potential in that location. The external energy of a control vertex is the sum of the average external energies derived from the corresponding patches from the three iso-parametric curves. Therefore, we obtain the following formulas for the external energy and external force of the control vertex P_{kji},

$$\begin{aligned}
E_{ext}(P_{kji}) = \ & \frac{1}{L}\sum_{l=0}^{L-1} E_{ext}(\sum_{i=0}^{I} S_{kji}B(\tfrac{u_i+u_{i-1}}{2} + l\ step_u))+ \\
& \frac{1}{M}\sum_{m=0}^{M-1} E_{ext}(\sum_{j=0}^{J} S_{kji}B(\tfrac{v_j+v_{j-1}}{2} + m\ step_v))+ \\
& \frac{1}{N}\sum_{n=0}^{N-1} E_{ext}(\sum_{k=0}^{K} S_{kji}B(\tfrac{w_k+w_{k-1}}{2} + n\ step_w)) \\
F_{ext}(P_{kji}) = \ & \frac{1}{L}\sum_{l=0}^{L-1} F_{ext}(\sum_{i=0}^{I} S_{kji}B(\tfrac{u_i+u_{i-1}}{2} + l\ step_u))+ \\
& \frac{1}{M}\sum_{m=0}^{M-1} F_{ext}(\sum_{j=0}^{J} S_{kji}B(\tfrac{v_j+v_{j-1}}{2} + m\ step_v))+ \\
& \frac{1}{N}\sum_{n=0}^{N-1} F_{ext}(\sum_{k=0}^{K} S_{kji}B(\tfrac{w_k+w_{k-1}}{2} + n\ step_w))
\end{aligned}$$

where $step_v = \frac{v_{j+1}-v_{j-1}}{2M}$, $step_w = \frac{w_{k+1}-w_{k-1}}{2N}$ and M and N are given constants.

References

[1] A. A. Amini, "Energy Minimizing Deformable Grids for Tracking Tagged MR Cardiac Images", In *Proceedings of Computers in Cardiology*, October, 1992, pp.651-654.

[2] A. A. Amini and et al., "MR Physics-Based Snake Tracking and Dense Deformations from Tagged MR Cardiac Images (oral presentation)", In *AAAI Symposium on Applications of Computer Vision to Medical Image Processing*, March, Stanford University, California, 1994.

[3] A. Amini, R. Curwen and J. Gore, "Snakes and Splines for Tracking Non-Rigid Heart Motion", In *European Conference in Computer Vision*, April, Cambridge University, UK, 1996.

[4] L. Axel and L. Dougherty, "MR Imaging of Motion with Spatial Modulation of Magnetization", *Radiology*, Vol.171, No.3, pp.841-845, 1989.

[5] L. Axel, R. C. Goncalves and D. Bloomgarden, "Regional Heart Wall Motion: Two-Dimensional Analysis and Functional Imaging with MR Imaging", *Radiology*, Vol. 183, 1992, pp.745-750.

[6] E. Bardinet, L. D. Cohen and N. Ayache, "A Parametric Deformable Model to Fit Unstructured 3D Data", Tech. Report No. 2617, INRIA, Sophia-Antipolis, Juliet, 1995.

[7] R. Bartels, J. Beatty and B. Barsky, "An Introduction to Splines for Use in Computer Graphics and Image Modelling", *Morgan Kauffmann: San Mateo*, CA, 1987.

[8] L. D. Cohen and I. Cohen, "Finite-Element Methods for Active Contour Models and Balloons for 2-D and 3-D Images", *IEEE Trans. PAMI*, Vol. 15, No. 11, pp. 1131-1147, 1993.

[9] W. Grossman, "Assessment of Regional Myocardial Function", JACC, Vol.7, No.2, 1986, pp. 327-328.

[10] A. Gueziec and N. Ayache, "Smoothing and Matching of 3-D Space Curve", International Journal of Computer Vision, Vol. 12, No. 1, 1994, pp. 79-104.

[11] A. Gueziec, "Surface Representation with Deformable Splines: Using Decoupled Variables", *Scientific Visualization*, Spring, 1995, pp.69-80.

[12] S. Gupta and J. Prince, "On Variable Brightness Optical Flow For Tagged MRI", In *Information Processing in Medical Imaging (IPMI)*, pp.323-334, 1995.

[13] M. A. Guttman, J. L. Prince and E. R. McVeigh, "Tag and Contour Detection in Tagged MR Images of the Left Ventricle", *IEEE Transactions on Medical Imaging*, 1994.

[14] R. M. Haralick and L. G. Shapiro, "The Facet Model," *Computer and Robot Vision, Vol.1,* Addison-Wesley, New York, 1992.

[15] M. Kass, A. Witkin and D. Terzopoulos, "Snakes: Active Contour Models," In *Proceedings of International Conference on Computer Vision*, pp.259-268, London, 1987.

[16] D. L. Kraitchman, A. A. Young, C.-N. Chang and L. Axel, "Semi-Automatic Tracking of Myocardial Motion in MR Tagged Images", *IEEE Trans. Med. Imaging*, Vol. 14, No. 3, 1995.

[17] S. Kumar and D. Goldgof, "Automatic Tracking of SPAMM Grid and the Estimation of Deformation Parameters from Cardiac MR Images", *IEEE Trans. Med. Imaging*, Vol. 13, 1994.

[18] F. Leymarie and M. D. Levine, "Fast Raster Scan Distance Propagation on the Discrete Rectangular Lattice", *CVGIP: IMAGE UNDERSTANDING*, Vol.55, No.1, pp.84-94, 1992.

[19] T. McInerney and D. Terzopoulos, " A Dynamic Finite Element Surface Model for Segmentation and Tracking in Multidimensional Medical Images with Application to Cardiac 4D Image Analysis", *Computerized Medical Imaging and Graphics*, Vol. 19, No. 1, 1995, pp. 69-83.

[20] S. Menet, P. Saint-Marc and G. Medioni, "B-Snakes: Implementation and Application to Stereo", In *Proceedings of DARPA Image Understanding Workshop*, Pittsburgh, 1990.

[21] C. C. Moore, W. G. O'Dell, E. R. McVeigh and E. A. Zerhouni, "Calculation of Three-Dimensional Left Ventricular Strains from Biplanar Tagged MR Images", *Journal of Magnetic Resonanse Imaging* , Vol. 2, No. 2, 1992, pp. 165-175.

[22] M. E. Mortenson, "Geometric Modeling", *John Wiley and Sons*, New York, 1985.

[23] E. N. Nilson, J. H. Ahlberg and J. L. Walsh, "The Theory of Splines and Their Applications", *Academic Press: New York*, 1967.

[24] W. G. O'Dell, C. C. Moore, W. C. Hunter, E. A. Zerhouni and E. R. McVeigh, "Three-Dimensional Myocardial deformations: Calculation with Displacement Field Fitting to Tagged MR Images", *Radiology*, Vol. 195, 1995, pp. 829-835.

[25] T. O'Donell, A. Gupta and T. E. Boult, "Periodic Generalized Cylinder Model with Local Deformations for Tracking Closed Contours Exhibiting Repeating Motion", In *Proc. of 12th IAPR ICPR* , Vol. A, Jerusalem, October 9-13, 1994, pp. 397-402.

[26] J. Park, D. Metaxas, A. Young and L. Axel, "Model-based Analysis of Cardiac Motion from Tagged MRI Data", In *Proc. of VII Annual IEEE Symp. on CBMS* , June 10-11, 1994.

[27] J. Park, D. Metaxas and L. Axel, "Volumetric Deformable Models with Parameter Functions: A New Approach to the 3D Motion Analysis of the LV from MRI-SPAMM", In *Proceedings of ICCV* , MIT, Cambridge, Massachusetts, US, June 20-23, 1995, pp. 700-705.

[28] J. Prince and E. McVeigh, "Motion Estimation from Tagged MR Image Sequences", In *IEEE Transactions on Medical Imaging*, Vol.11, No.2, June, pp.238-249, 1992.

[29] P. Radeva, J. Serrat and E. Martí, "A Snake for Model-Based Segmentation", In *Proceedings of ICCV* , Cambridge, Massachusetts, June 20-23, 1995, pp. 816-821.

[30] Keith R. Symon, "Mecanica", *Aguilar*, Madrid, 1970.

[31] D. Terzopoulos, J. Platt, A. Barr and K. Fleisher, "Elastically Deformable Models", *Computer Graphics*, Vol. 21, No. 4, July, 1987, pp. 205-214.

[32] D. Terzopoulos and D. Metaxas, "Dynamic 3D Models with Local and Global Deformations: Deformable Superquadrics", *IEEE Trans. PAMI* , Vol. 13, No. 7, July, 1991, pp. 703-714.

[33] A. Young and L. Axel, "Three-Dimensional Motion and Deformation of the Heart Wall: Estimation with Spatial Modulation of Magnetization - A Model-based Approach", *Radiology*, Vol. 185, 1992, pp.241-247.

[34] A. A. Young, D. L. Kraitchman and L. Axel, "Deformable Models for Tagged MR Images: Reconstruction of Two- and Three-Dimensional Heart Wall Motion", In *Proceedings of IEEE Workshop on Biomedical Image Analysis*, Seattle, WA, June, 1994, pp.317-323.

[35] A. A. Young, D. L. Kraitchman, L. Dougherty and L. Axel, "Tracking and Finite Element Analysis of Stripe Deformation in Magnetic Resonance Tagging", In *IEEE Transactions on Medical Imaging*, Vol. 14, No. 3, September, 1995, pp. 413-421.

[36] E. Zerhouni, D. Parish, W. Rogers, A. Yang and E. Shapiro, "Human Heart: Tagging with MR Imaging – A Method for Noninvasive Assessment of Myocardial Motion", *Radiology*, Vol.169, pp.59-63, 1988.